J. Fluid Mech. (2002), *vol.* 472, *pp.* 211–228.
DOI: 10.1017/S0022112002002252 Printed in the United Kingdom

Dynamics of vortices on a uniformly shelving beach

By L. R. CENTURIONI†

Southampton Oceanography Centre, European Way, Southampton, SO14 3ZH, UK

(Received 11 May 2001 and in revised form 25 February 2002)

Laboratory experiments are described which investigate the dynamics of a vortex dipole moving in water towards a planar sloping beach inclined at an angle α to the horizontal. Results are compared with those of a vortex ring model first developed by Peregrine (1996). The vortices separate as they travel up the beach, eventually moving in opposite directions and nearly parallel to the shoreline. The ranges of conditions examined are $3^\circ \leqslant \alpha \leqslant 45^\circ$, $1 \times 10^3 \leqslant Re \leqslant 6 \times 10^3$ and $0.05 \leqslant Fr \leqslant 0.14$, where Re and Fr are the on-slope Reynolds number and the Froude number of the vortices, respectively. The minimum distance from the shoreline reached by the vortices and their along-shore speed are in general agreement with the predictions when, respectively, $R_i^* < 3$ (where R_i^* is the non-dimensional initial distance of the vortices from the shore-line) and $Re \gtrsim 1500$. The vortex ring model is likely to have useful applications to the study of the dynamics of the near-shore zone.

1. Introduction

Horizontal dispersion and mixing in the ocean is frequently associated with the dynamics of coherent vortices. This study was motivated by the desire to describe the motion of vortices in a near-shore environment, where the sea surface and an approximately planar sloping beach define a wedge of fluid in which the vortices are moving. The Rossby number of the vortices, $\Omega/\pi f$ (e.g. Tritton 1988, p. 217, where Ω is the angular velocity of the core, assuming rigid rotation, and f is the Coriolis parameter), is $\gg 1$ and they are not affected by the rotation of the Earth. Observations of such vortices are rare (but see Smith & Largier 1995), a consequence of the limitations of the available measurement techniques. In contrast, many numerical experiments have predicted how such vortices develop as a result of instabilities of along-shore currents (e.g. see Dodd, Iranzo & Reiners 2000; Özkan-Haller & Kirby 1999; Slinn, Allen & Holman 2000). Peregrine (1998) noted that the surf zone is a highly turbulent region that continuously receives energy from breaking waves and, since the flow there can be regarded as almost two-dimensional, an inverse energy cascade may lead to the formation of coherent vortices. Recent work by Buhler & Jacobson (2001) has shown how vortex dipoles may be generated by an inhomogeneous wavetrain impinging on a barred beach. The vortex dipole is then self-advected towards the shoreline.

A method of describing such vortices has been suggested by Peregrine (1996). Consider a wedge formed by a horizontal plane, the sea surface, and one inclined at an angle, α, to the horizontal, the seabed. The planes meet along a line, the apex of

† Present address: Scripps Institution of Oceanography, La Jolla, CA 92093-0213, USA: lcenturioni@ucsd.edu

the wedge, which we shall call the shoreline. Circular vortex rings with zero swirl and with axes lying along the shoreline satisfy conditions of zero flow normal to the two planes, and consequently the parts of the vortex rings lying outside the wedge form the 'image' system of the parts of the vortices in a 'real' water-filled fluid between the sea surface and the seabed (Peregrine 1996, 1998; Thorpe & Centurioni 2000). The interaction of two (or more) such vortices in a wedge is consequently identical to that of the same number of smoke rings sharing a common axis. Hicks (1922) reported the first systematic study on the interaction of pairs of vortex rings.

The present paper describes laboratory experiments designed to test the extent to which this model of vortices may apply in reality and provide useful estimates of vortex motion. In the experiments vortex pairs are directed up a sloping plane normal to the shoreline. They subsequently separate and move apart roughly parallel to the shoreline, and their speeds and positions are compared to predictions.

2. Theory

A circular line vortex with small but finite cross-section area and uniform ω/l inside the core, where ω is the vorticity and l is the distance from the axis of symmetry, moves, without deformation, along its axis with a finite and constant speed v, given by

$$v = \frac{\Gamma}{4\pi R}\left\{\log\frac{8R}{r} - \frac{1}{4} + \left(\frac{r}{R}\right)^2\left[-\frac{3}{8}\log\frac{8R}{r} + \frac{15}{32}\right] + o\left(\left(\frac{r}{R}\right)^4\log\frac{8R}{r}\right)\right\} \qquad (1)$$

(Fraenkel 1972; Saffman 1992, p. 199 equation 16). Γ is the strength of the vortex (see Saffman 1992, p. 8 for a definition), r is the radius of its approximately circular cross-section and R is the radius of the ring.

Consider two equal, non-viscous, thin-cored and co-axial vortex rings of radius R_i and opposite sign so that they repel one another, separated by a distance s_i. As the two vortices move apart the radii of the rings decrease (Lamb 1932, art. 164, describes the opposite situation for which the two rings approach one another and the radii increase). We wish to calculate the constant final radius of the rings, R_f, when they have moved infinitely apart and therefore, since isolated, move in opposite directions at an equal and constant speed (as given by equation (1)). This system is Hamiltonian and therefore its kinetic energy, or Hamiltonian function, is conserved (Saffman 1992, pp. 206–207 and equation 9):

$$E_i + E_i^{12} = E_f, \qquad (2)$$

where E_i is the initial kinetic energy of the two isolated vortices, E_i^{12} is the initial interaction kinetic energy for the couple and E_f is the final kinetic energy of the two isolated vortices. Note that when the vortices are far apart the interaction kinetic energy term can be neglected, as shown later. Throughout the work, the subscripts 'i' and 'f' refer to the initial and final situations respectively. The kinetic energy of a sector α of an isolated vortex ring with constant ω/l inside the core is given by (e.g. Saffman 1992, p. 199)

$$E_s(\Gamma, R, r, \alpha) = \frac{\Gamma^2 R}{2}\left\{\log\frac{8R}{r} - \frac{7}{4} + \cdots\right\}\frac{\alpha}{2\pi}, \qquad (3)$$

and therefore, if (2) is applied to the wedge of fluid of angular amplitude α and the symmetry of the system is exploited, E_i and E_f, which now refer to the sectors of the

rings, can be expressed as

$$E_i = 2E_s(\Gamma, R_i, r_i, \alpha), \tag{4}$$

$$E_f = 2E_s(\Gamma, R_f, r_f, \alpha). \tag{5}$$

If the two rings have an approximately circular cross-section, the initial and final radius of the core are related by the equation of the conservation of volume of a torus:

$$r_f = r_i \left(\frac{R_i}{R_f}\right)^{1/2}. \tag{6}$$

The interaction kinetic energy of the vortex pair, E_i^{12}, considering again only two sectors of angular amplitude α of the rings, can be calculated by the equation (e.g. Saffman 1992, p. 207)

$$E_i^{12} = \frac{\alpha}{2\pi}\left[\pi \int \omega_+ \psi_- \, \mathrm{d}A_+ + \pi \int \omega_- \psi_+ \, \mathrm{d}A_-\right], \tag{7}$$

where $\omega_{+(-)}$ is the vorticity of the positive (negative) vortex, $\psi_{-(+)}$ is the Stokes stream function of the negative (positive) vortex and the integrals are restricted to the regions containing the positive (negative) vorticity, i.e. over the core of the positive (negative) vortex. The two surface integrals in (7) are calculated over any half-plane stemming from the axis of symmetry (Batchelor 1967, p. 521, equation 7.2.11). Since the system is axisymmetric and the two vortices are equal (but with opposite signs), the two integrals in (7) are also equal, resulting in

$$E_i^{12} = \alpha \int \omega_+ \psi_- \, \mathrm{d}A_+ = \alpha \int \omega_- \psi_+ \, \mathrm{d}A_-. \tag{8}$$

The Stokes stream function of, for example, a negative circular vortex filament, at a generic point $P = (x, \rho)$ in an axial plane, is (Lamb 1932, art. 161, equation 11)

$$\psi_-(x, \sigma) = -\frac{\Gamma}{2\pi}(l_1 + l_2)[\mathrm{K}(\lambda) - \mathrm{E}(\lambda)], \tag{9}$$

where l_1 and l_2 are the distances of P from the two centres of the cross-sections, say $c_1 = (s_i/2, R_i)$ and $c_2 = (s_i/2, -R_i)$, on the axial plane, that is,

$$l_1 = \sqrt{(x - s_i/2)^2 + (\rho - R_i)^2}, \tag{10}$$

and

$$l_2 = \sqrt{(x - s_i/2)^2 + (\rho + R_i)^2}, \tag{11}$$

and λ is expressed as

$$\lambda = \frac{l_2 - l_1}{l_2 + l_1}. \tag{12}$$

K and E are the complete elliptic integrals of first and second kind, respectively. If the initial distance between the two vortices, s_i, is large enough to neglect the variations of ψ_- over the area of integration, which is a good approximation if $s_i \gg r_i$, and using the definition of strength, equation (8) becomes

$$E_i^{12} = \alpha \int \omega_+ \psi_- \, \mathrm{d}A_+ \approx \alpha \psi_- \int \omega_+ \, \mathrm{d}A_+ = \alpha \psi_- \Gamma. \tag{13}$$

The explicit form of the interaction kinetic energy is obtained by substituting (9),

calculated for example at the point $(-s_i/2, R_i)$, into (13), that is,

$$E_i^{12} = -\frac{\alpha\Gamma^2}{2\pi}(s_i + \sqrt{s_i^2 + 4R_i^2})[\mathrm{K}(\lambda) - \mathrm{E}(\lambda)], \tag{14}$$

where λ is now given by

$$\lambda = \frac{\sqrt{s_i^2 + 4R_i^2} - s_i}{\sqrt{s_i^2 + 4R_i^2} + s_i}. \tag{15}$$

The interaction kinetic energy of the two rings, equation (14), tends to zero with λ, which is equivalent to s_i becoming infinite. In other words, vortices that are very far apart have zero interaction kinetic energy. This justifies the fact that the right-hand side of (2) does not contain a term analogous to (14). Substituting (4), (5) and (14) into (2), we obtain

$$R_i\left[\log\left(\frac{8R_i}{r_i}\right) - \frac{7}{4}\right] - (s_i + \sqrt{s_i^2 + 4R_i^2})[\mathrm{K}(\lambda) - \mathrm{E}(\lambda)] = R_f\left[\log\left(\frac{8R_f^{3/2}}{r_i R_i^{1/2}}\right) - \frac{7}{4}\right], \tag{16}$$

where r_f has been eliminated with (6). Equation (16) is independent of Γ, the strength of the vortices, and of α, the angular amplitude of the wedge of fluid. It relates the final radius of the rings, R_f, to their initial radius, R_i, their initial distance, s_i, and the initial radius of their core, r_i.

Hicks (1922) has given the equation for the trajectory followed by two equal vortex rings with opposite sign. The same result can be obtained from equation (16) if we observe that, for example, the left-hand term must be constant throughout the motion of the vortices. The constant is determined by the appropriate initial conditions and the path can be computed numerically from (16) with the aid of (6) to eliminate the dependence from the radius of the cross-section.

These results, namely equations (1) and (16), apply to complete vortex rings as well as to circular sectors of them in a wedge of fluid, or, equivalently, to our idealized 'beach'. Therefore, we have estimates of the distance of the vortex centres from the shoreline and their along-shore speeds when they are far apart. Equations (1) and (16) are, however, valid only if two rigid planes with no associated boundary layers bound the wedge of fluid. If the upper surface is free, a cylindrical body of fluid with circular cross-section of radius r in solid-body rotation with angular velocity Ω (i.e. with vorticity $\omega = \Omega/2$, and therefore strength $\Gamma = \pi\omega r^2$) produces a depression at the centre of $(\frac{1}{8}\pi^2 g)\Gamma^2/r^2$, where g is the acceleration due to gravity. A Froude number, defined as

$$Fr = \frac{\Gamma^2}{8\pi^2 g r^2 h} \tag{17}$$

(e.g. Tritton 1988, p. 95; Thorpe & Centurioni 2000), where h is the characteristic water depth, must therefore be $\ll 1$ if the rigid-surface assumption is valid.

3. The apparatus and the experiments

Experiments were carried out in the Perspex tank sketched in figure 1 (Centurioni 2000). A wedge of free-surface water was created by installing a glass panel, a 'beach', inclined at an angle α to the horizontal (with α ranging from $\sim 3.5^\circ$ to $\sim 45^\circ$). Barker & Crow's (1977) design of the vortex generator was used (see Centurioni 2000 for more experimental details). The dipoles, generated over the flat bottom,

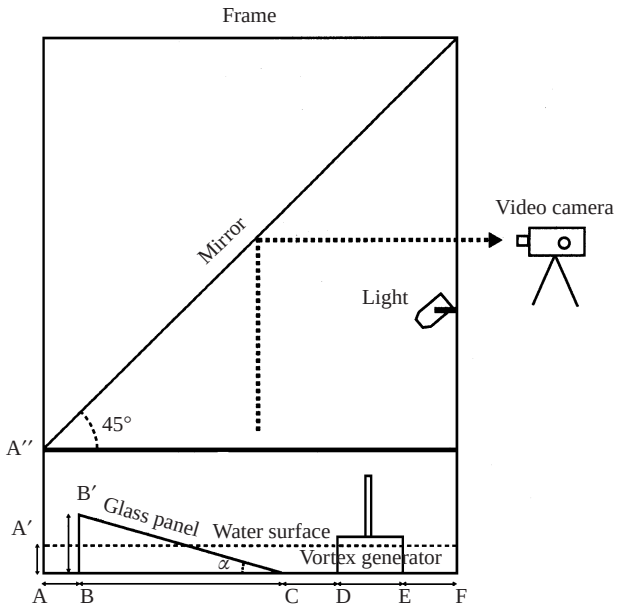

FIGURE 1. The experimental tank. The sketch shows a side view. The tank width is 1470 mm. AF = 970 mm, AA″ = 250 mm, DE = 120 mm, EF = 160 mm, CD = 110 mm. The width of the sloping plane, B′C, is varied together with BB′ to obtain different inclinations, α. The vortex generator is in the middle of the longest side of the tank. A metallic frame holds a mirror at 45° to the horizontal. The 50 Hz shutter video camera (Cohu Cosmicar TV zoom lens, 8–48 mm f1.2 and Rainbow TV zoom lens H6X8–II, 8–43 mm f1.0) points at the mirror to record a view from above of the water surface. Further details are given in Centurioni (2000).

progress at 90° towards the shoreline, the intersection of the water surface with the beach. The vortex generator was driven by a weight sliding over a lubricated sloping plane so that the pushing plate of the vortex generator moved with approximately constant speed. A strong solution of yellow fluorescein was injected into the channel of the vortex generator immediately before each run to make the vortices visible. The images, recorded on tapes with a 50 Hz shutter video camera, were used to measure the position of the centre of the vortices. The particle image velocimetry (PIV) technique (Adrian 1991) was also used to: (*a*) visualize features of the flow; (*b*) measure the position of the vortices; and (*c*) measure the velocity (and vorticity) field. Before each experiment, the surface of the fluid was seeded with white granules of the astyrene/acrylate interpolymer Pliolite AC 80 with diameters in the ranges 500–710 μm or 710–1000 μm. The velocimetry analysis was performed with the software DIGIMAGE (Dalziel 1993). Tables 1 and 2 show the range of slope angles and off-slope depths used for the experiments with dye and with particles. The constriction of the lateral walls should result in an offshore speed of the vortices of about 10^{-1} cm s^{-1}. This estimate is based on a strength of the dipole $\Gamma \sim 150\,\mathrm{cm^2\,s^{-1}}$, separation of the vortices $s \sim 50$ cm and distance from the shoreline $R \sim 15$ cm.

Figure 2 shows a time series of pictures from an experiment with fluorescein. The motion of the dipole can be divided in four main phases: (i) after the generation, at $t = 0$, and while on the flat bottom, the vortices move parallel to each other and with a slowly increasing separation along a straight path ($0 < t < 4$ s); (ii) when the vortices meet the slope, at $t = t_1$ (~ 6 s), while still progressing towards the shoreline, they separate more rapidly until they reach a minimum distance (R_f) from the shoreline

Exp.	α (deg.)	h (cm)	Γ_i (cm^2 s^{-1})
1	3.5	2.7	94 ± 36
2	5.5	2.5	101 ± 32
3	5.5	4.5	105 ± 33
4	7.0	2.5	79 ± 34
5	7.0	4.5	129 ± 41
6	8.5	2.5	89 ± 33
7	8.5	4.5	106 ± 28
8	10.0	2.5	96 ± 29
9	10.0	4.5	134 ± 39
10	12.0	2.5	80 ± 31
11	12.0	4.5	104 ± 28
12	18.0	4.5	114 ± 34
13	20.0	4.5	117 ± 40
14	45.0	4.5	104 ± 37

TABLE 1. Values of the nominal slope angle, α, and the nominal water level, h (the depth of the water at the flat bottom region). For this set of experiments fluoroscein was used as tracer. Γ_i, the initial strength is defined by (18).

Exp.	α (deg.)	h (cm)	Γ_i (cm^2 s^{-1})
15	3.5	2.7	127 ± 18
16	5.5	2.5	89 ± 10
17	5.5	4.5	N/A
18	7.0	2.5	114 ± 20
19	7.0	4.5	188 ± 22
20	8.5	2.5	107 ± 13
21	8.5	4.5	160 ± 20
22	10.0	2.5	77 ± 11
23	10.0	4.5	201 ± 9
24	12.0	2.5	89 ± 14
25	12.0	4.5	133 ± 13
26	18.0	4.5	93 ± 11

TABLE 2. As table 1, for the PIV experiments. Γ_i is calculated from vorticity measurements (see the Appendix).

at $t = t_2$ (~ 14 s); (iii) then the vortices move parallel to the shoreline and apart from each other ($14 < t < 34$ s); (iv) at $t = t_3$ (~ 34 s) they start to move towards deeper water. For vortices impacting on a vertical wall similar stages of development occur (Barker & Crow 1977; van Heijst & Flor 1989; Orlandi 1990). The offshore movement of the vortices (stage iv) is referred to as rebounding and is seen by comparing the two images in figure 2 at $t = 28$ s and $t = 46$ s. Maximum rebound speeds are typically 0.3 cm s^{-1}, and always larger than the speeds of the off-shore motion associated with the impermeable lateral walls discussed earlier. The four phases can be identified in figure 3, where the position of the two vortices is plotted together with the path followed by two thin-cored sectors of vortex rings calculated numerically from (16).

Because of the diffusion of the fluorescein, the details of the centres of the vortices are lost in the first few seconds, making the subsequent identification of their positions difficult. Streak photographs give a clearer view of the flow at the fluid surface as shown in figures 4 and 5. The trajectories of the particles provide information about

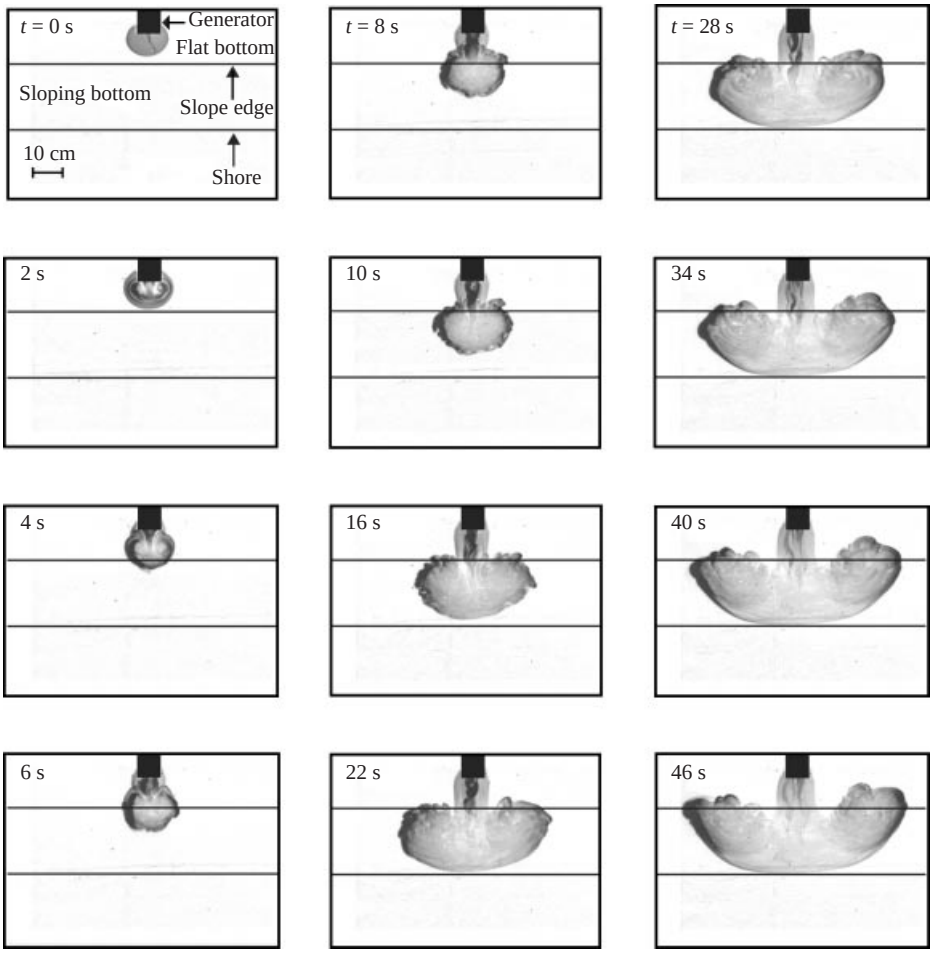

FIGURE 2. The evolution of a vortex dipole (experiment 4 in table 1) progressing over the flat horizontal bottom (from $t = 0$ s to $t_1 \sim 4$ s) and subsequently over the planar slope. The images are a plan view of the flow from above. The positions of the shoreline and of the edge of the slope are indicated in the first frame. The vortices are coloured with fluorescein and a black background was used to enhance the contrast. These images were obtained after: (*a*) the use of an interlace filter; (*b*) the subtraction of the background (as recorded before the run); (*c*) the conversion to negative. The vortices reach the minimum distance from the shoreline at $t_2 \sim 14$ s. Rebounding starts approximately at $t_3 \sim 34$ s. The water depth at the flat bottom is (2.7 ± 0.1) cm and the angle of the planar slope to the horizontal is $\alpha = 7.0° \pm 0.1°$. The strength of the incident dipole, as calculated from its speed over the flat bottom, is $\Gamma = (79 \pm 34)\,\mathrm{cm^2\,s^{-1}}$. The pictures show only part of the domain.

the structure of the flow. The secondary vortices, marked by filled arrows, contribute to the rebounding process.

There was evidence that the flow associated with the vortices was generally turbulent. The series of pictures in figure 2 show how the outer border of the dipole passes through different phases, starting with an apparently smooth laminar flow during the roll-up of the vortices (at $t = 2$ s), which becomes irregular (for $t \geqslant 6$ s) and eventually laminar again as the fluid slows down (for $t > 22$ s). The inner core of the vortices can also be turbulent. Small eddies, indicated by hollow arrows, appear at the surface and

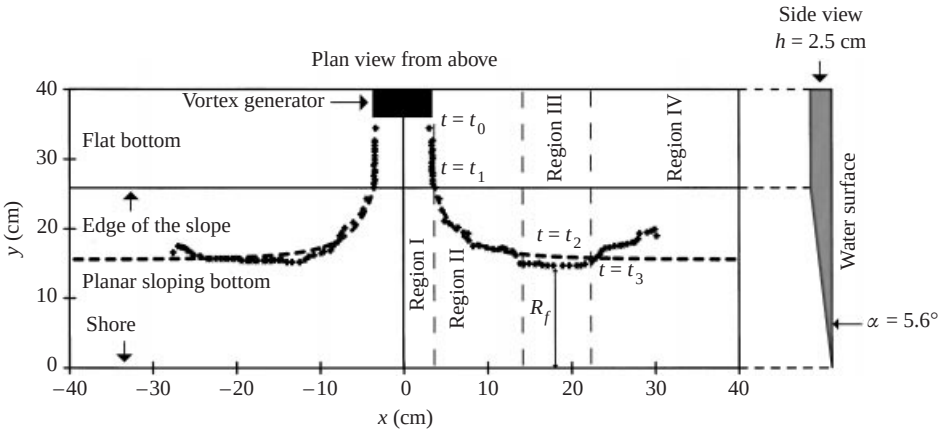

FIGURE 3. The position of the two vortices (experiment 2, table 1). The planar slope is at an angle $\alpha = (5.6 \pm 0.1)^\circ$ to the horizontal. The water depth at the flat bottom, h, is (2.5 ± 0.1) cm. The position is marked every 0.4 s before the centre of the vortices meets the slope and 0.8 s afterwards. The three vertical dashed lines define four regions in which the vortices behave differently (only the right-hand side has been marked). When the vortices are in region I, they progress on a straight path and their separation is constant or slowly increasing. When the vortices enter region II, they are over the sloping bottom and their separation increases as they progress towards the shoreline. Region III is characterized by the minimum position (R_f) of the vortices from the shoreline. Finally (region IV), the secondary vortices (not shown) generated by the viscous interaction of the main flow with the boundary become strong enough to move the primary vortices offshore (rebounding, but the lateral walls may contribute to it). The path followed by two thin-cored sectors of vortex rings (thick dashed line) is superimposed and was calculated by solving numerically (16) with the following initial conditions: $R_i = 26.9$ cm, $s_i = 6.8$ cm and $r_i = 3.4$ cm. The dependence on the radius of the cross-section was eliminated with (6).

near the centre of rotation in figure 4, between $t = 6$ s and $t = 12$ s. After the dipole crosses the edge between the flat bottom and the slope, the vortices, so far circular and with only one centre of rotation, change shape and appear to have two distinct centres of rotation. Far from the centres of rotation the streamlines are elliptical (with eccentricity $e \sim 0.5$ at $t = 6$ s to $e \sim 0.7$ at $t = 10$ s). At $t = 16$ s the streamlines in the proximity of the centre of the vortices again become almost circular.

4. Measurements

In the experiments with fluorescein the position of the centre of each vortex was measured from its image, and its strength was computed (see table 1) from its relationship with the speed of a vortex dipole over a flat bottom:

$$v = \frac{\Gamma_i}{2\pi s_i} \tag{18}$$

(Batchelor 1967, p. 531) where Γ_i is the strength of the dipole and s_i is the distance between the centres of the two vortices.

The PIV technique is ideal for generating streak photographs but involves bias if used to measure the position of the centres of the vortices and correction is needed (see the Appendix). The total amount of vorticity at the surface of the fluid measured with the PIV experiments (integral (A3) estimated with a vorticity threshold of 0 and separated into four components, two for the main vortices and two for the secondary vortices) was used to normalize (we considered 90%, 95% and 99% of the total

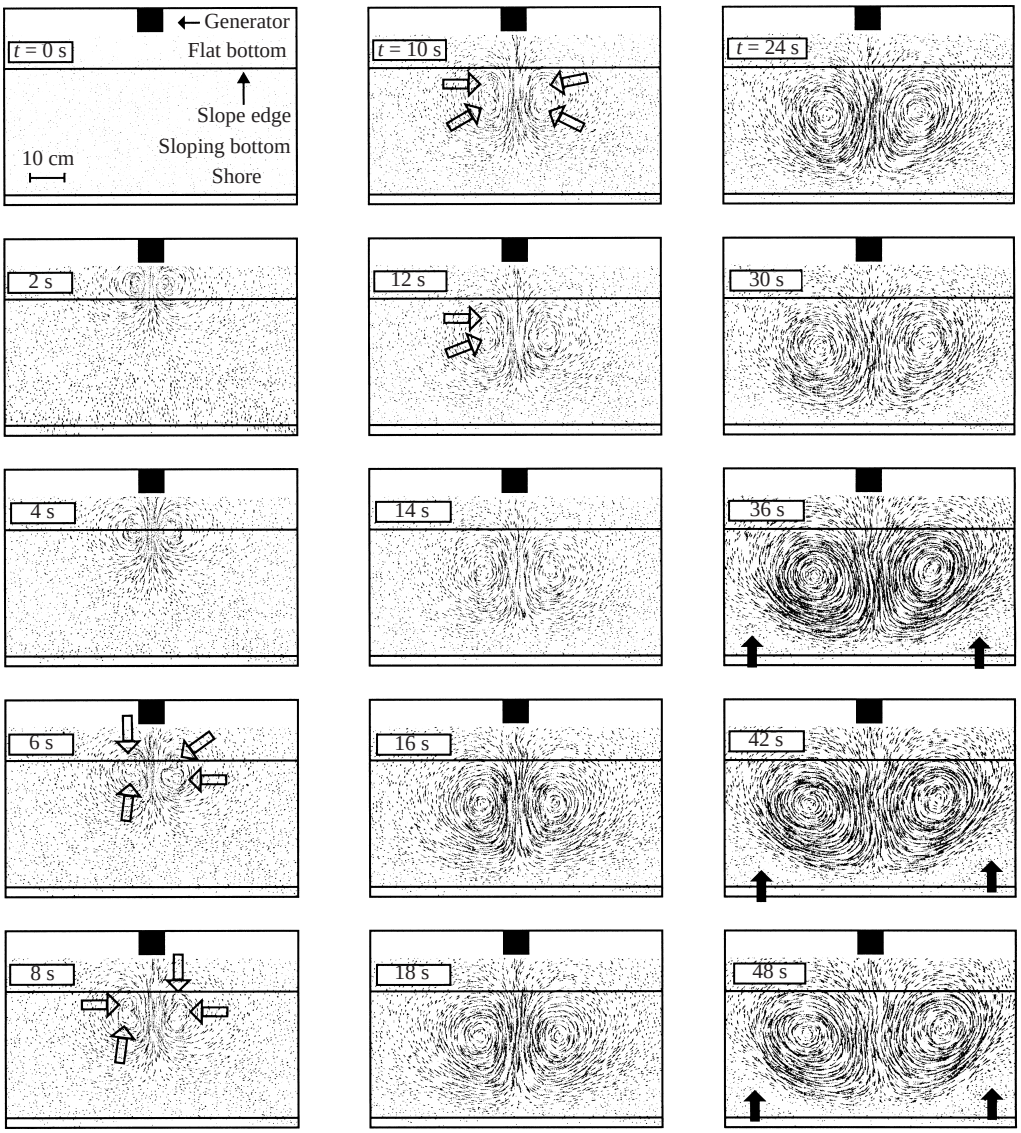

FIGURE 4. A time series of streak photographs in a plan view from above (PIV technique, experiment 15 in table 2). The exposure time for frames from 0 s to 16 s was ~ 0.8 s, ~ 1.6 s from 16 s to 24 s and ~ 3.2 s from 26 s to 30 s. The images do not show all the particles used to seed the fluid but only those that satisfied criteria imposed by the PIV analysis. The water depth at the flat bottom is (2.7 ± 0.1) cm and the angle formed by the planar slope with the horizontal is $\alpha = (3.4 \pm 0.1)^\circ$. The strength of the dipole measured over the flat bottom is $\Gamma = (127 \pm 18)\,\mathrm{cm^2\,s^{-1}}$, and decreases to $\Gamma = (90 \pm 13)\,\mathrm{cm^2\,s^{-1}}$ when the vortices move parallel to the shoreline. Hollow arrows mark multiple centres of rotation in the core of the vortices. Weak secondary vortices, marked by filled arrows, develop. The images show only part of the domain.

vorticity) the calculated strengths of the main and secondary vortices. The relative accuracy of the vorticity field at the water surface measured by the PIV technique was taken as 10% (Linden, Boubnov & Dalziel 1995). The average time series of the normalized strengths were calculated. The initial strength of the dipole Γ_i was averaged over an interval, typically about 2 s, centred around t_1, the instant at which

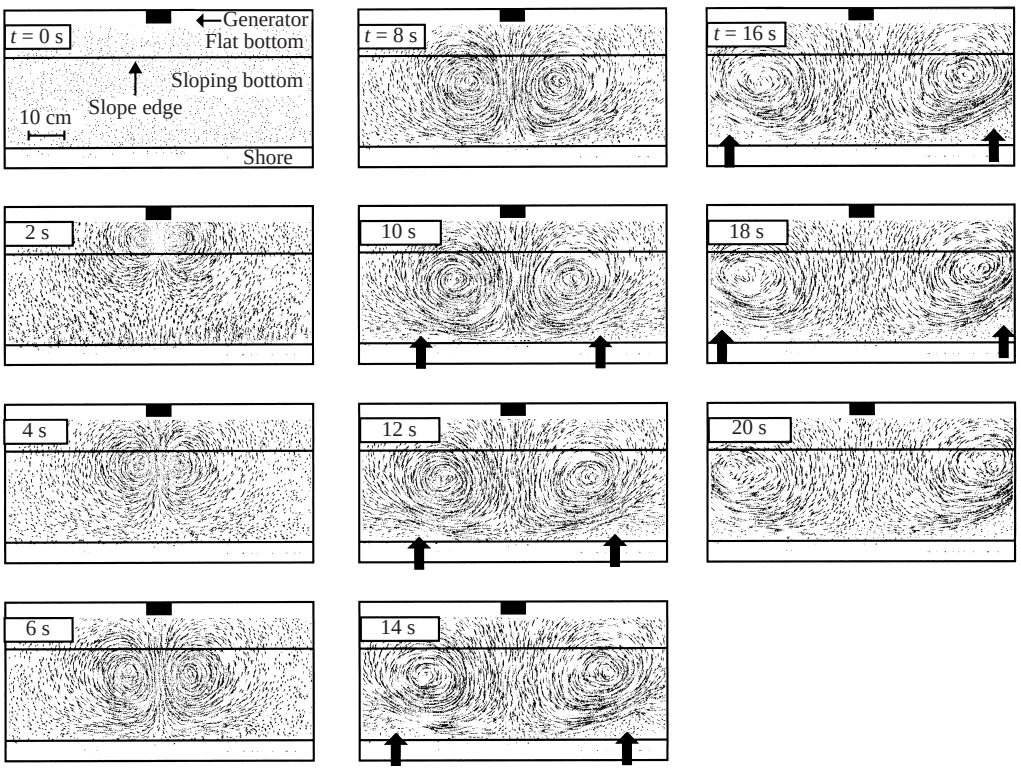

FIGURE 5. Streak photographs from experiment 23 in table 2 as in figure 4. The exposure time for frames from 0 s to 6 s is $\sim$ 1 s and for frames from 8 s to 20 s is $\sim$ 2 s. The water depth at the flat bottom is (4.6 ± 0.1) cm and the angle formed by the planar slope with the horizontal is $\alpha = (9.8 \pm 0.2)^\circ$. The strength of the dipole over the flat bottom is $\Gamma = (201 \pm 9)\,\mathrm{cm^2\,s^{-1}}$ and decreases to $\Gamma = (186 \pm 13)\,\mathrm{cm^2\,s^{-1}}$ when the vortices move parallel to the shoreline. The images show only part of the domain.

the vortices cross the edge, at a horizontal distance R_i from the shoreline, between the flat bottom and the planar slope (table 2). Γ_f, the strength of the vortices at the minimum distance from the shoreline, R_f, was also estimated and ranged between $71\,\mathrm{cm^2\,s^{-1}}$ and $185\,\mathrm{cm^2\,s^{-1}}$).

Care was taken to obtain estimates of the initial radius of the vortices. A parameter, r_{99}, proportional to the area S_{99} containing 99% of the total vorticity,

$$r_{99} = \sqrt{\frac{S_{99}}{\pi}}, \tag{19}$$

was computed. This represents the radius of the core of the vortex if the vorticity is contained in a circular surface. Similarly, we defined and computed r_{90} and r_{95}. The three time series were averaged into one, from which estimates of the radii, r_i and r_f, were taken, respectively, when the vortices were at distances R_i and R_f from the shoreline; r_i ranged from 4.4 cm to 6.1 cm and r_f ranged from 6.8 cm to 11.1 cm. The radius of the core of the secondary vortices was estimated in a similar way.

The minimum distance of the vortices from the shoreline during the along-shore motion (phase iii, see e.g. figure 3), R_f, was measured from the averaged path of

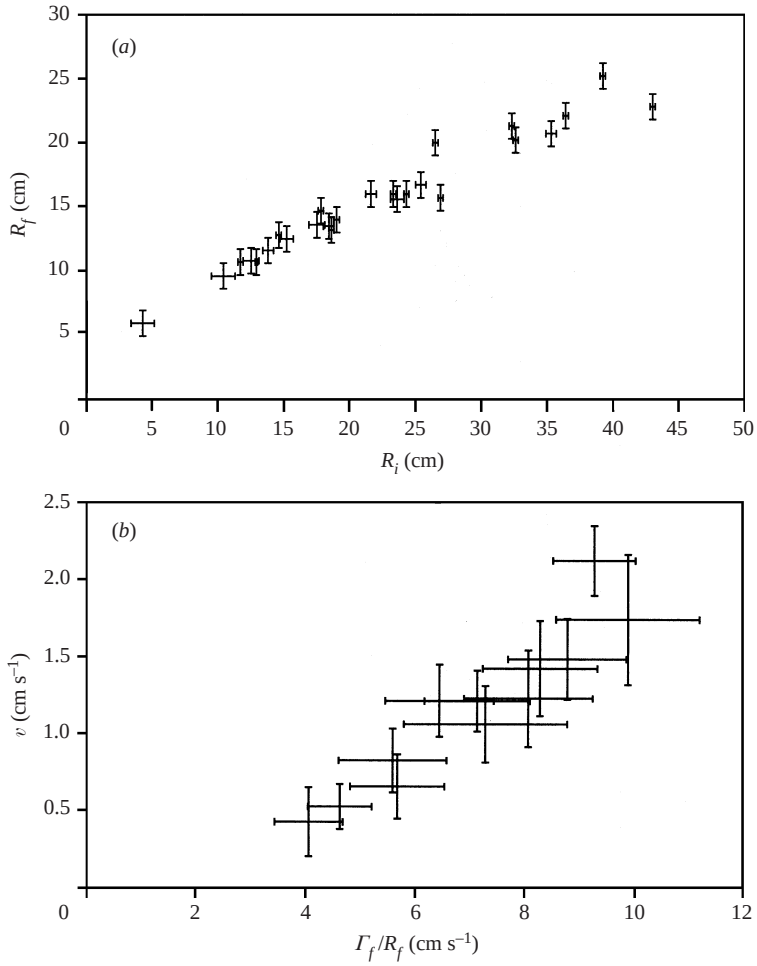

FIGURE 6. (*a*) The minimum distance from the shoreline reached by the vortices (R_f) versus the distance of the edge of the planar slope from the shoreline (R_i) in the horizontal plane. (*b*) Averaged along-shore velocities of the vortices, v, versus the ratio of the strength (Γ_f) to the minimum distance of the vortices from the shoreline (R_f).

the positive and negative vortices, and values are shown in figure 6(*a*), plotted against R_i. We computed the corresponding speed v of an isolated vortex moving over the planar slope in the direction parallel to the shoreline, but in the PIV experiments only. Values are shown in figure 6(*b*), plotted against the ratio Γ_f/R_f.

5. Comparison of the inviscid theory with observations

We now compare the measured values of R_f with the predictions of (16). The distance between the vortices, s_i, was used to define the non-dimensional quantities:

$$R_i^* = \frac{R_i}{s_i}, \quad r_i^* = \frac{r_i}{s_i}, \quad R_f^* = \frac{R_f}{s_i}. \tag{20a,b,c}$$

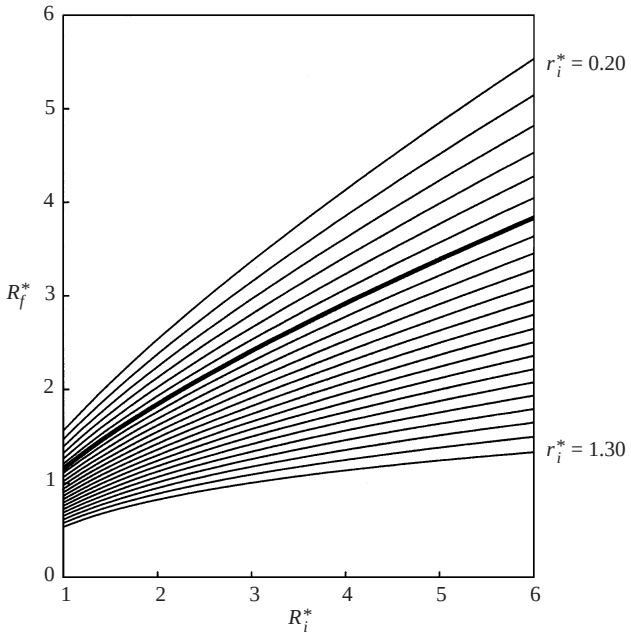

FIGURE 7. Solutions of (21) for r_i^* in 0.05 intervals between 0.2 and 1.3. The condition $R_i^* = 1$ means that the initial radius of the rings is equal to their initial separation and the condition $r_i^* = 0.5$ (bold line) means that the initial radius of the cross-sections of the vortices is half their separation.

Equation (16) becomes

$$R_i^* \left(\log 8 \frac{R_i^*}{r_i^*} - \frac{7}{4} \right) - (1 + \sqrt{1 + 4(R_i^*)^2})[\mathrm{K}(\lambda^*) - \mathrm{E}(\lambda^*)] = R_f^* \left\{ \log \left[8 \frac{R_f^*}{r_i^*} \left(\frac{R_f^*}{r_i^*} \right)^{1/2} \right] - \frac{7}{4} \right\}, \quad (21)$$

with,

$$\lambda^* = \frac{\sqrt{1 + 4(R_i^*)^2} - 1}{\sqrt{1 + 4(R_i^*)^2} + 1} = \lambda. \quad (22)$$

Equation (21) was solved numerically for $R_i^* \in [1, 6]$ and $r_i^* \in [0.2, 1.3]$ (figure 7). The relationship between R_f^* and R_i^* becomes less sensitive to r_i^* when the latter increases and R_i^* is small. Since we could not measure r_i in the experiments with fluorescein we started with the assumption $r_i^* = r_i/s_i = 0.5$ for all the experiments. The results, plotted in figure 8(a), show that for almost all the experiments except numbers 1 and 14, for which the agreement is remarkable, the theoretical predictions systematically overestimate the observations (although the majority of the experimental data are consistent with the predictions if the error bars are taken into account). The ratio μ, defined as the relative difference between the final theoretical kinetic energy and the final experimental kinetic energy, that is,

$$\mu = \frac{E_f(R_i^*, R_{f,t}^*, r_i^*) - E_f(R_i^*, R_{f,e}^*, r_i^*)}{E_f(R_i^*, R_{f,t}^*, r_i^*)} \quad (23)$$

(here E_f is the term on the right of (21), $R_{f,t}^*$ is the non-dimensional final distance from the shoreline predicted by (21) and $R_{f,e}^*$ is measured from the experiments)

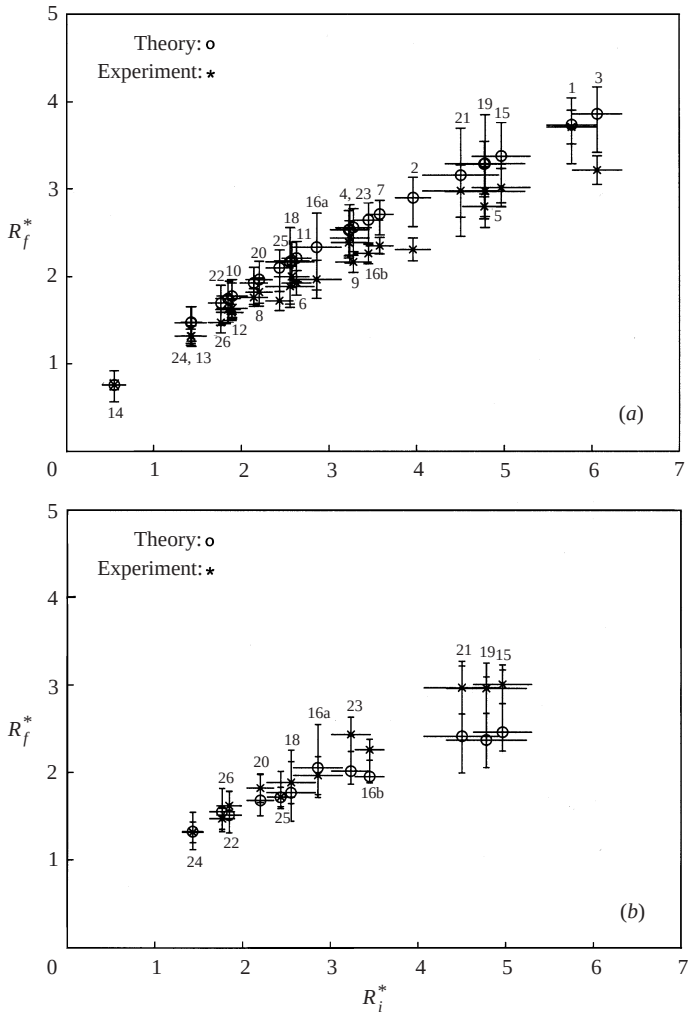

FIGURE 8. The experimental non-dimensional final distance from the shoreline, R_f^*, plotted as a function of the initial non-dimensional distance from the shoreline, R_i^*, and compared with the predictions of equation (21). In (*a*) $r_i = 2s_i$, whilst in (*b*) r_i is the measured value (PIV experiments only). The numbers relate to experiments listed in tables 1 and 2.

was used to quantify the agreement between theory and observations since $\mu = 0$ when $R^*_{f,t} = R^*_{f,e}$. The ratio μ was always positive and averaged 0.5. By restricting the analysis to the PIV experiments we were able to use the measured values of r_i. The improved agreement, figure 8(*b*), is confirmed by an average absolute value of μ of 0.3.

The speed of the vortices during the along-shore motion was compared with the predictions of (1). The analysis was restricted to the PIV experiments since only then were we able to measure the strength and the radius of the vortices on the slope. Equation (1) can be rewritten as

$$v = \frac{\Gamma_f}{4\pi R_f}\left\{\log\frac{8}{\varepsilon_f} - \frac{1}{4} + \varepsilon_f^2\left[-\frac{3}{8}\log\frac{8}{\varepsilon_f} + \frac{15}{32}\right] + o\left(\varepsilon_f^4 \log\frac{8}{\varepsilon_f}\right)\right\}, \tag{24}$$

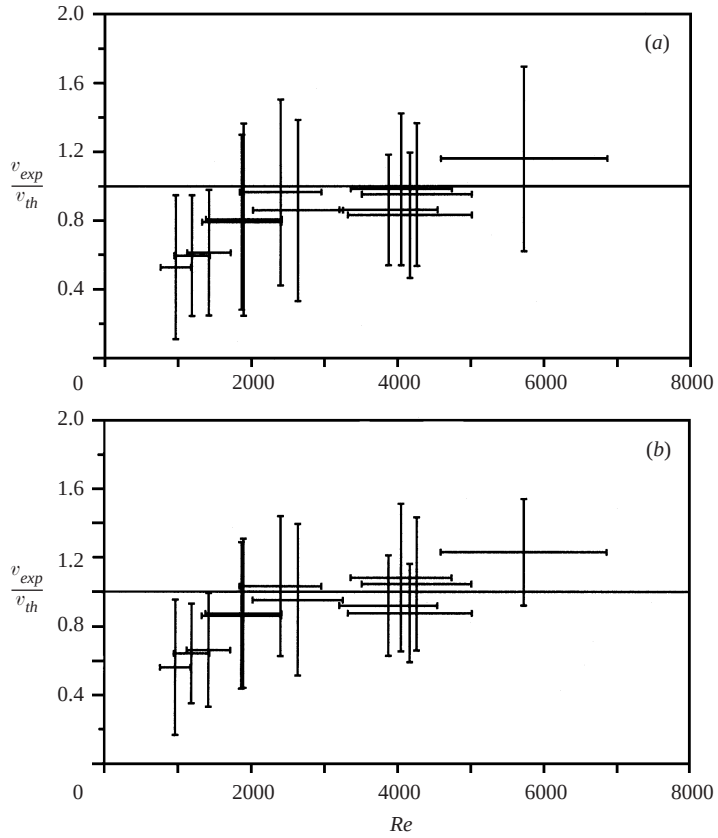

FIGURE 9. The ratio of the observed and theoretical along-shore speed of the vortices (respectively, v_{exp} and v_{th}) plotted as a function of the Reynolds number, Re. Comparison of the averaged experimental data with: (a) the predictions of equation (24); (b) the predictions of Norbury's (1973) model. The agreement between theory and experiments is, in both cases, within the error bounds when $Re > Re_b$, with $Re_b \sim 1500$.

where

$$\varepsilon_f = \frac{r_f}{R_f}. \tag{25}$$

Equation (24) is valid if $\varepsilon_f \ll 1$ (Fraenkel 1972; Saffman 1992, pp. 195–201) and, if applied to the wedge of fluid, suggests that the along-shore speed of the vortices is independent of the angle of the planar slope. Norbury (1973) calculated the speed of a family of rings ranging from thin cored rings ($\varepsilon = 0.1$) to Hill's spherical vortices ($\varepsilon = \sqrt{2}$), thus including the case in which the condition $\varepsilon_f \ll 1$ is violated, as it is in our experiments where ε_f ranges from 0.5 to 0.7. Figure 9 shows the ratios between the experimental speed and either (a) the predictions of equation (24) or (b) Norbury's (1973) model plotted as a function of the Reynolds number, here defined as

$$Re = \frac{\Gamma_f}{r_f}\frac{h_s}{\nu}, \tag{26}$$

where h_s is the local water depth and $\nu = 0.011\,\mathrm{cm^2\,s^{-1}}$ is the kinematic viscosity of water (e.g. Batchelor 1967). Both models overestimate the experimental data for Reynolds numbers less than Re_b, with $Re_b \sim 1500$, but the agreement is within the error bounds of the estimated values for larger values of Re.

6. Discussion

Figure 8(*b*) suggests that the agreement of the experimental data with the theory deteriorates for values of R_i^* exceeding 3 (experiments 23, 16b, 21, 19 and 15, although the agreement is still within the error bounds), where predictions of the length R_f underestimate the observations. These are the experiments in which the vortices have travelled for longer across the bathymetric contours and for which bottom friction effects may be important. These are also the experiments for which the width of the slope in the horizontal, R_i^*, is largest and for which the vortical fluid is contained almost entirely in the wedge region during the along-shore motion. Our theory is valid when the sloping plane extends to infinity. However, the experiments show that even when part of the vortical flow is outside the wedge region during the along-shore motion, the agreement is within the estimated errors. Furthermore, experiments 23, 21, 19 and 15 have the largest initial Froude numbers ($0.1 \leqslant Fr \leqslant 0.3$ for the PIV experiments), which indicate the most significant departures from the rigid lid approximation.

Equation (16) requires that the strength of the vortices is conserved and the radius of the core is governed by (6). Time series of these two parameters show that up to 30% of the initial circulation of the main vortices is lost before they become well-separated from one another (the largest losses are observed when $Re \lesssim 1500$) and that r_f cannot be completely explained by (6). In addition, viscosity and turbulent bed friction are a likely cause of the observed secondary vortices (figures 4 and 5) that extract energy from the main vortex dipole. If we write $\Gamma_f = \eta\Gamma_i$ (in which $\eta < 1$ represents a loss of strength) and (6) is not used, (21) may be rewritten as

$$R_i\left[\log\left(\frac{8R_i}{r_i}\right)-\frac{7}{4}\right]-(s_i+\sqrt{s_i^2+4R_i^2})[\mathrm{K}(\lambda)-\mathrm{E}(\lambda)] = \eta^2 R_f\left[\log\left(\frac{8R_f}{r_f}\right)-\frac{7}{4}\right]. \quad (27)$$

This holds as before if energy is not dissipated or transferred to other motions. The energy associated with the observed secondary flow, estimated using the formula for the kinetic energy for a Hill's spherical vortex (e.g. Saffman 1992, p. 199) is found to be about 1% of the estimated initial energy of the system (i.e. the left-hand term of (2)), and can sensibly be neglected in the energy balance. Equation (27) has limited applications since it appears difficult to predict η and r_f^* in terms of the initial conditions, or, in other words, to model the evolution of the vorticity, as discussed by Buhler & Jacobson (2001) who refer to the case of a horizontal bottom. The presence of a sloping bottom adds additional complexity. However, if measured values of η and r_f are used, (27) can serve as a test for these ideas, for then μ averages 0.2 (ranging from 0.007 for experiment 18 to 0.38 for experiment 21).

With regard to the along-shore speed of the vortices (figure 9), it is difficult to find anything other than a dependence on the Reynolds number as an explanation of the differences between observations and predictions. The on-slope Froude number of the vortices (ranging from 0.05 to 0.14) does not appear to have any influence. A dependence on other factors, such as the slope angle, is possible, although, given the design of the experiments, we were unable to test this hypothesis, which remains open to further research. The conclusion is 'robust' in that it is not sensitive to the definitions of the strength and radius of vortices – the results obtained for the 90th, 95th and 99th percentiles, equation (19), were all consistent – nor it is sensitive to the time interval used for the averaging operations.

The theory presented here requires the flow to be two-dimensional, i.e. to lie entirely in planes passing through the shoreline, the common axis of the image vortex rings.

However, vertical motions were observed and consisted mainly of (a) a vortex with its horizontal axis at the forefront of the dipolar structure, which was observed to dissipate once the vortices start to move apart and (b) upward vertical motions of the order of $\sim 1\,\mathrm{cm\,s^{-1}}$ inside the core of the vortices during phase (i) (flat bottom). The vortex generator may be responsible for (a), which in turn might be responsible for some of the differences between theory and observations seen in figure 8(b). Given the transient character of this flow structure however, it seems unlikely that this should affect the analyses of the along-shore speeds (the use of a tank with a rigid lid, see Barker & Crow 1977, might lead to the elimination of this horizontal vortex, although requiring a more complicated apparatus). The motions inside the vortex core (b) certainly play a role in modifying the vorticity distribution. The PIV technique as used here is limited in that it can only look at the surface of the fluid. These vertical motions are probably responsible for an increase of the radius of the cores of the vortices beyond that predicted by equation (6). Since the rate of change of the radius of the vortices is highest at the beginning of the experiments we suggest that vertical motions may be relatively unimportant in the analysis of the along-shore speed of the vortices, v, while they may play a role in R_f.

Our formulation of the problem is based on a theory valid for thin-cored rings for which the ratio ω/l is constant in the core. Our experiments suggest that the vorticity distribution has a maximum roughly coincident with the position of the stagnation point and a bell shape. Fraenkel (1970, 1972) has shown that for a form of the vorticity distribution with a maximum at the stagnation point, the parameter $-1/4$ in (1), obtained for constant ω/l, increases to 0. A more detailed investigation of the agreement between the theory and the experiments will require a better knowledge of the distribution of ω.

7. Conclusions

A theory is proposed which is useful in describing the motion of an inviscid and two-dimensional vortex dipole in a wedge of fluid. Laboratory experiments were carried out to test its validity as a vortex dipole propagates into shoaling water.

The flow followed qualitatively the same phases of evolution as those of a vortex dipole approaching a vertical wall at normal incidence (Barker & Crow 1977). Rebounding was observed, with typical speeds of about $0.3\,\mathrm{cm\,s^{-1}}$, although a contribution from the rigid lateral walls may be envisaged. The flow was generally three-dimensional.

The comparison of the experiments with the predictions of the final distance from the shoreline (R_f^*, equation (21)) shows an agreement that is generally within the experimental errors. If the measured values of the initial radius of the vortices are used the agreement is always within the error bounds and remarkably good when R_i^* is less than 3. When the along-shore speed of a vortex is compared with the predictions of the vortex-ring theory the agreement is within the experimental errors if Re is greater than about 1500, that is, when the losses of strength of the main vortices are lowest.

The experimental results show that the vortex-ring theory provides accurate predictions of along-shore propagation of vortices, especially at high Reynolds numbers, and may therefore be useful in interpreting observations in the surf-zone, as previously suggested. Many aspects deserve further research, such as the decay of a viscous vortex in the presence of bottom friction on a sloping plane (see Buhler & Jacobson 2001). Experiments conducted with a wider range of slope angles and Reynolds numbers would provide further tests and insights into the limitations of the theory.

Professor Steve Thorpe is gratefully acknowledged for his continuous support and for directing my attention towards the vortex-ring theory. I wish to thank Professor D. W. Moore for his comments on the manuscript and for drawing my attention on the role of the distribution of vorticity. Dr Gregg Lane-Serff provided support with the laboratory experiments and Mr Ray Collins built the vortex generator. Constructive comments from two referees and a revision of the text by Dr Carl Amos and Mr Alan Hughes are gratefully acknowledged. Pliolite AC 80 was kindly provided by Goodyear. Partial funding for this research was provided by the University of Southampton, UK.

Appendix

The centre of rotation seen by an observer fixed with respect to the tank (the apparent centre of rotation) differs from the one seen by another observer moving (but not rotating) with the vortex since the first will see the superposition of the rotational motion around the centre and the translational motion of the vortex whilst the second sees only the rotation of the vortex. The distance between the two centres depends on the translational speed of the vortex and on its vorticity distribution. Saffman (1979) studied a similar situation. He calculated the trajectories of the apparent centre of rotation, of the true centre of rotation and the changes in shape for a symmetric and two-dimensional vortex dipole approaching a vertical wall. The true centre of rotation, or centroid, of the two-dimensional vortex, say (x_0, y_0), is defined as (Saffman 1979)

$$x_0 = \frac{\int_0^\infty \int_0^\infty y\omega \, \mathrm{d}x \, \mathrm{d}y}{\Gamma}, \tag{A 1}$$

$$y_0 = -\frac{\int_0^\infty \int_0^\infty x\omega \, \mathrm{d}x \, \mathrm{d}y}{\Gamma}, \tag{A 2}$$

where $\omega(x, y)$ is the vorticity and Γ is the strength of the vortex, that is,

$$\Gamma = \int_0^\infty \int_0^\infty \omega \, \mathrm{d}x \, \mathrm{d}y. \tag{A 3}$$

From the vorticity field (PIV analysis) we estimated, using finite sums, the integrals (A 1), (A 2) and (A 3). To do this one possibility is to define *a priori* the regions of the fluid containing the vortices and then estimate the integrals over this area. A second possibility is to consider only the vorticity values above, for positive vorticity, or below, for negative vorticity, a certain threshold and then repeat the procedure for a number of thresholds. We used the second method, briefly outlined below, since it does not require a definition of the boundary of the vortices. The integrals were estimated for the following set of thresholds: $\pm 12.0\,\mathrm{s}^{-1}, \pm 11.9\,\mathrm{s}^{-1}, \ldots, \pm 0.1\,\mathrm{s}^{-1}, \pm 0.05\,\mathrm{s}^{-1}, 0\,\mathrm{s}^{-1}$. Since the flow, at least at the surface, is approximately symmetric throughout the duration of the experiments (figures 2, 4 and 5), the fluid domain was split in two regions along the axis of symmetry of the flow ($x = 0$ in figure 3). For each threshold value the vorticity (and the regions) forming the two main vortices and the two secondary vortices was selected. The resulting 244 trajectories were averaged into one single path. The same procedure was used to track the movement of the secondary vortices. Among all the experiments, the greatest difference between the two measurements of R_f, that is from manual analysis of streak pictures and from the integral method just described, was $(16 \pm 3)\%$.

REFERENCES

Adrian, R. J. 1991 Particle-imaging techniques for experimental fluid mechanics. *Annu. Rev. Fluid Mech.* **23**, 261–304.

Barker, S. J. & Crow, S. C. 1977 The motion of two-dimensional vortex pairs in a ground effect. *J. Fluid Mech.* **82**, 659–671.

Batchelor, G. K. 1967 *An Introduction to Fluid Dynamics*. Cambridge University Press.

Buhler, O. & Jacobson, T. E. 2001 Wave-driven currents and vortex dynamics on barred beaches. *J. Fluid Mech.* **449**, 313–339.

Centurioni, L. R. 2000 Dynamics of near-shore vortices. PhD Thesis, University of Southampton.

Dalziel, S. 1993 *Digimage, Image Processing for Fluid Dynamics. Installation Guide, System Overview & Particle Tracking*. Cambridge Environmental Research Consultants Ltd.

Dodd, N., Iranzo, V. & Reniers, A. 2000 Shear instabilities of wave-driven alongshore currents. *Rev. Geophys.* **38**, 437–463.

Fraenkel, L. E. 1970 On steady vortex rings of small cross-section in an ideal fluid. *Proc. R. Soc. Lond.* A **316**, 29–62.

Fraenkel, L. E. 1972 Examples of steady vortex rings of small cross-section in an ideal fluid. *J. Fluid Mech.* **51**, 119–135.

van Heijst, G. J. F. & Flor, J. B. 1989 Laboratory experiments on dipole structures in a stratified fluid. In *Mesoscale/Synoptic Coherent Structures in Geophysical Turbulence* (ed. J. C. J. Nihoul & B. M. Jamart), pp. 591–608. Elsevier.

Lamb, H. 1932 *Hydrodynamics*, 6 edn. Cambridge University Press.

Linden, P. F., Boubnov, B. M. & Dalziel, S. B. 1995 Source-sink turbulence in a rotating stratified fluid. *J. Fluid Mech.* **298**, 81–112.

Norbury, J. 1973 A family of steady vortex rings. *J. Fluid Mech.* **57**, 417–431.

Orlandi, P. 1990 Vortex dipole rebound from a wall. *Phys. Fluids* A **2**, 1429–1436.

Özkan-Haller, T. H. & Kirby, J. T. 1999 Nonlinear evolution of shear instabilities of the longshore current: a comparison of observations and computations. *J. Geophys. Res.* **104**, 25953–25984.

Peregrine, D. H. 1996 Vorticity and eddies in the surf-zone. In *Coastal Dynamics 95* (ed. W. R. Dally & R. B. Zeidler), pp. 460–464. ASCE.

Peregrine, D. H. 1998 Surf zone currents. *Theoret. Comput. Fluid Dyn.* **10**, 295–309.

Saffman, P. G. 1979 The approach of a vortex pair to a plane surface in inviscid fluid. *J. Fluid Mech.* **92**, 497–503.

Saffman, P. G. 1992 *Vortex Dynamics*. Cambridge University Press.

Slinn, D. N., Allen, J. S. & Holman, R. A. 2000 Alongshore currents over variable beach topography. *J. Geophys Res.* **105**, 16971–16988.

Smith, J. A. & Largier, J. L. 1995 Observations of nearshore circulation: rip currents. *J. Geophys. Res.* **100**, 10967–10975.

Thorpe, S. A. & Centurioni, L. R. 2000 On the use of the method of images to investigate near-shore dynamical processes. *J. Mar. Res.* **58**, 779–788.

Tritton, D. J. 1988 *Physical Fluid Dynamics*, 2nd edn. Clarendon.